Results in Physics 7 (2017) 813–822

Contents lists available at ScienceDirect

Results in Physics

journal homepage: www.journals.elsevier.com/results-in-physics

Applying the Network Simulation Method for testing chaos in a resistively and capacitively shunted Josephson junction model

Fernando Gimeno Bellver [a], Manuel Caravaca Garratón [a], Antonio Soto Meca [a], Juan Antonio Vera López [a], Juan L.G. Guirao [b], Manuel Fernández-Martínez [a,*]

[a] University Centre of Defence at the Spanish Air Force Academy, MDE-UPCT, C/Coronel López Peña s/n, 30720 Santiago de la Ribera, Murcia, Spain
[b] Technical University of Cartagena, Department of Applied Mathematics and Statistics, Hospital de Marina, 30203 Cartagena, Spain

ARTICLE INFO

Article history:
Received 23 July 2016
Received in revised form 22 December 2016
Accepted 30 January 2017
Available online 4 February 2017

Keywords:
Electrical analogy
Network Simulation Method
Josephson junction
Chaos indicator
Fast Fourier Transform

ABSTRACT

In this paper, we explore the chaotic behavior of resistively and capacitively shunted Josephson junctions via the so-called Network Simulation Method. Such a numerical approach establishes a formal equivalence among physical transport processes and electrical networks, and hence, it can be applied to efficiently deal with a wide range of differential systems.

The generality underlying that electrical equivalence allows to apply the circuit theory to several scientific and technological problems. In this work, the Fast Fourier Transform has been applied for chaos detection purposes and the calculations have been carried out in PSpice, an electrical circuit software.

Overall, it holds that such a numerical approach leads to quickly computationally solve Josephson differential models. An empirical application regarding the study of the Josephson model completes the paper.

Introduction

Circuit theory has an undeniable attractive to deal with physical dynamical systems described via differential equations. The analogy among physical systems and electrical networks is a well-known academic subject [1,2] whose usefulness is especially highlighted in the context of complex nonlinear systems. In this way, a powerful method following that methodology and being based on circuit theory, is the so-called Network Simulation Method (NSM), a numerical approach applied to design electrical network models equivalent to certain transport processes and also for simulation purposes, by applying a suitable software for electrical circuit analysis [3]. Its power and efficiency could be employed to easily deal with the simulation of an electrical device having some complex nonlinear dynamics: the Resistively and Capacitively Shunted Josephson Junction (RCSJ, hereafter).

The Josephson junction (JJ) is a well-known technological application of superconductivity in electronics. It consists of a simple macroscopic quantum-mechanical device with a pair of superconductor layers linked by an insulating barrier allowing the quantum tunnel effect [4,5]. Cooper pairs at both sides of the insulator could be represented by wave functions that permeate the insulator via the tunnel effect and lock their phases to a constant value. Then a current proportional to the sinus of the phase difference between both sides of the junction is generated [6]. This system tends to give rise to nonlinear effects in its electromagnetic behavior. Thus, it becomes possible to explore chaotic dynamics in the junction behavior in experiments and in simulations, as well [7]. Moreover, due to the simplicity underlying its mathematical model, it could be applied to similar nonlinear dynamical systems. A detailed knowledge regarding the nonlinear dynamic and non-equilibrium effects in this superconducting system becomes necessary to understand some applications of the derived superconducting devices: SQUIDs, phase detectors, microwave or terahertz pulses generators [8], amplifier, transmitter and receiver in communications with chaos [9–11], to quote some of them. It is also worth noting that JJ resonators could produce chaotic signals in a wide range of frequencies [12].

For all these reasons, the JJ has become a test case in the study of chaos [13,14], experimentally and in simulations [15], both digital and analogic [16], due to their fundamental and practical interest [10]. The understanding and synchronization of chaotic systems becomes relevant in a great number of complex physical [17], chemical, biological, and even economic and social systems, or applications having finite transmission times [18], variable

* Corresponding author.
E-mail address: manuel.fernandez-martinez@cud.upct.es (M. Fernández-Martínez).

http://dx.doi.org/10.1016/j.rinp.2017.01.041
2211-3797/

switching speed and memory effects, and turbulent and unpredictable behaviors [19].

Along the last decades, the interest for those systems has grown increasingly. Indeed, chaos can be used to mask, transmit, filter and recover encoded information in the chaotic carrier wave [20–25], and to generate cryptographic keys [26], as well. The JJ model can be applied to simulate those systems under similar mathematical models such as nonlinear optical devices, the Belousov–Zhabotinsky chemical reaction or Rayleigh–Bénard convection cells [27], and to study how tuning the parameters can lead to or avoid chaos.

The theoretical behavior of the JJ has been classically modeled via RL or RCL electric circuits [28], where the parameters are considered to be constants (standard JJ models). However, for a more realistic description regarding the behavior of the system, these parameters should also depend on some variables including temperature, external magnetic field, or even dimensions and profile of the junctions, among others [29]. We shall refer to them as generalized JJ models, hereafter.

It is also worth mentioning that the dynamics of the JJ model have been extensively studied via several numerical methods [30]. Overall, the design and solution of analogic electrical networks constitute a fundamental alternative to classic numerical approaches. Blackburn [31] designed an electronic analogic circuit for a RCSJ in which no analog switches are required and high performance op-amp were used to reduce the noise and improve the bandwidth. Vicent et al. [32] explored the control and synchronization of chaos in the RLC shunted Josephson junction by means of a backstepping design after solving the model with the Matlab/Simulink block.

In this paper, we contribute an alternative method based on the NSM, a numerical approach based on the formal equivalence between physical transport processes and electrical networks. A universal and equivalent electrical network is designed starting from the mathematically set of coupled differential equations. Each term in the differential equations, whatever its expression, is modeled as an appropriate current branch implemented in the network model via a certain electrical device. This is interconnected with the rest of them under the Kirchhoff current law (KCL), according to the sign of the addends in the equation. Accordingly, the NSM establishes a natural equivalence between physical transport currents and electrical currents. Further, since the network only contains a few devices (a resistor, a capacitor, and a voltage-controlled current source, see forthcoming Section '*The generalized RCSJ model. Dependence of the critical current on an external magnetic field*'), the network design becomes quite easy and can be run in a circuit computer code such as PSpice.

Hence, no further mathematical manipulation is required since the remaining work is carried out by the algorithms in the simulation code. It has been proved that the contributed model, which can be run in a PC with relatively short computing times, becomes a powerful and precise tool to study a great variety of problems [33–41]. This constitutes one of the main advantages of the NSM.

Moreover, since the simulation code assumes the KCL, the balance of the flow variables (conservation law) is inherently assured without adding new requirements to the model. Thus, the user is not required neither to manipulate the large set of algebraic differential equations nor to pay special attention to its convergence, due to the sophisticated numerical procedures integrated in the circuit simulation codes.

On the other hand, a powerful tool to test for chaotic dynamics in nonlinear systems is the Fast Fourier Transform (FFT), also included in PSpice. The Fourier spectrum of a signal is one of the most applied chaos measures in dynamical systems by scientists and engineers [42]. The chaotic signal presents a continuous distribution of frequency (broad band spectrum) in contrast to the periodic and quasi-periodic signals, which are characterized by the presence of discrete spikes.

In this paper, the results obtained after applying the NSM to some phenomena that appear in the JJ, including the intermittency and the chaotic behavior, are analyzed in both the standard and the generalized models. This has been carried out via the study of the phase diagrams and the spectral analysis of the FFT in PSpice. The standard model could still be solved using specific packages such as JSPICE. Nevertheless, if the parameters are no longer constant (as in the generalized model discussed along Section '*The generalized RCSJ model. Dependence of the critical current on an external magnetic field*'), then the complexity of the problem may quickly be increased and those packages become quite ineffective. Therefore, the novelty in this work mainly consists of the application of the NSM to efficiently deal with the generalized model. Additionally, some of the results have also been compared with those from some classical approaches in order to test for efficiency, reliability, and accuracy regarding the NSM.

The structure of this paper is as follows. In Section '*Theoretical Background*', we provide all the necessary preliminaries including the basics on Josephson junctions, the RCSJ model, the generalized RCSJ model, the NSM method, and the FFT, as well. Section '*Results and Discussion*' contains the results and the discussion, and finally, Section '*Conclusions*' summarizes the main conclusions for this work.

Theoretical background

Josephson junctions

When two superconducting elements are separated by a thin insulating film, it holds that the wave functions for both sides could be represented via the following expression [29,43]:

$$\psi_i = \sqrt{n_i} e^{j\theta_i} \quad i = 1, 2 \tag{1}$$

where n_i is the Cooper pairs density and θ_i denotes the wave function phase, as well. Further, both sides are coupled through the next equations:

$$\begin{aligned} j\hbar\dot{\psi}_1 &= \mu_1\psi_1 + K\psi_2 \\ j\hbar\dot{\psi}_2 &= \mu_2\psi_2 + K\psi_1 \end{aligned} \tag{2}$$

where $\mu_1 = -\mu_2 = \frac{2e \cdot V}{2}$ are the energy levels at both sides of the junction, V is the electrical potential between both sides, 2e is the Cooper pair electric charge, and K denotes the coupling constant, as well.

From both Eqs. (1) and (2), and separating the real and imaginary parts we obtain that

$$\begin{aligned} &\hbar\tfrac{\partial n_1}{\partial t} = -\hbar\tfrac{\partial n_2}{\partial t} = 2k\sqrt{n_1 n_2}\sin(\theta) \quad \theta = \theta_2 - \theta_1 \\ &-\hbar\tfrac{\partial(\theta)}{\partial t} = \mu_2 - \mu_1 \end{aligned} \tag{3}$$

where θ refers to the phase difference of the wave functions. Since the change rate of the density of Cooper pairs is the transport current across the junction, then the first expression in Eq. (3) leads to

$$I = \frac{\partial n_1}{\partial t} = -\frac{\partial n_2}{\partial t} = \frac{2k}{\hbar}\sqrt{n_1 n_2}\cdot\sin(\theta) = I_0 \sin\theta \tag{4}$$

where I_0 is the critical current of the superconducting junction. Moreover, the voltage across the junction from the second equality at Eq. (3) is given by

$$V = \frac{\hbar}{2e}\frac{\partial\theta}{\partial t} \tag{5}$$

These key expressions do govern the electric behavior of a JJ.

The standard RCSJ model

The model described above represents the ideal behavior of a JJ. However, the junctions behave more accurately according to an equivalent electrical model, namely, the RCSJ, also known as Steward-McCumber model [44,45]. Fig. 1 provides a graphical approach regarding the RCSJ for illustration purposes. It is also worth mentioning that the RCSJ is the most appropriate model to study both frequency and chaos [10,46,47].

In this scheme, R represents the unavoidable resistive derivation (shunt) that short-circuits the junction, and C is a capacitor, which takes into account the accumulated charge between the terminals of the JJ and causes displacement currents, as well. There is no classical equivalent for the JJ and it is usually denotes as X in the circuits. The first KCL yields the following total intensity expression:

$$I = C\frac{\partial V}{\partial t} + \frac{V}{R} + I_0 \sin\theta \tag{6}$$

The voltage V in this approach is governed by Eq. (5), in addition to the laws of behavior of both the resistor and the capacitor [48,49]. When R, C and I_0 remain constant, then Eq. (6) is known as the standard RCSJ model, which can be rewritten, using the flux quantum $\Phi_0 = \frac{h}{2e}$ as

$$I = C\Phi_0\frac{\partial^2\theta}{\partial t^2} + \frac{\Phi_0}{R}\frac{\partial\theta}{\partial t} + I_0\sin\theta \tag{7}$$

That expression is a second order differential equation having a nonlinear component. It can be rewritten in two dimensionless ways, where the normalized current is $i = I/I_0$. To deal with, one option is to consider the Josephson circle frequency, Ω_c [43]. In the present work, we have used another normalization, which is related with the plasma frequency, Ω_p. This can be stated as follows: let $\Omega_p = \sqrt{I_0/C\Phi_0}$, $\tau = \Omega_P t$ (normalized time), $\omega_P = \Omega/\Omega_P$(normalized frequency), $v = V/I_0R$ (normalized voltage), and $\gamma = 1/\Omega_P RC$ (damping parameter) [43]. Hence,

$$i = \frac{\partial^2\theta}{\partial\tau^2} + \gamma\frac{\partial\theta}{\partial\tau} + \sin\theta \tag{8}$$

Further, if the system is forced through an external AC intensity current, $i = A\sin(\omega\tau)$, where A is the amplitude and ω is the angular frequency, then the governing uncoupled equations are the following:

$$\begin{aligned} A\sin(\omega\tau) &= \tfrac{dv}{d\tau} + \gamma v + \sin\theta \quad (a)\\ v &= \tfrac{d\theta}{d}\tau \quad (b) \end{aligned} \tag{9}$$

These expressions will be applied in upcoming calculations for simulation purposes.

The generalized RCSJ model. Dependence of the critical current on an external magnetic field

Firstly, observe that Eq. (7) models the ideal JJ, where all the parameters remain constant in time. In general, both parameters C and R present a strong dependence on temperature T [50,51], as well as on other factors as aging [52], though the critical current I_C becomes the most revealing. In fact, this may even depend on the magnitude of an external magnetic field applied to the superconducting device. Thus, the generalized RCSJ model is represented again by Eq. (7), but notice that the parameters may vary due to the effect of a physical variable, such as temperature, external magnetic field, self-field effect, JJ dimensions and non-uniformity of the junction surface [53–57], non-linearity of R and parasitic inductances. From the above mentioned, temperature remains constant in applications, aging does not play a relevant role in our simulations due to the short time length windows we work with, and non-uniformity of the junction surface as well as JJ dimensions stand as a result from the fabrication procedure. In our study, nor the non-linearity of R or the parasitic inductances have been considered, though their effects could be explored in future research. Instead of this, we shall be focused on the effect of an external magnetic field, disregarding the self-field induced by the tunneling current.

If a uniform field B is applied parallel to the interphase plane of the samples (as shown in Fig. 2), the critical current exhibits a dependence described by the following expression [29]:

$$I_C = I_0\left|\frac{\sin\left(\frac{ed'LB}{\hbar}\right)}{\frac{ed'LB}{\hbar}}\right| \tag{10}$$

where I_0 is the value of the critical current in absence of the magnetic field, L is the lateral dimension of the sample perpendicularly to the direction of the applied field, and $d' = d + 2\lambda$ is the effective insulator thickness, with d and λ being the insulator thickness and the penetration depth, respectively. Eq. (10) could be simplified by defining the renormalized magnetic flux through the cross section by $\chi = 2\pi\Phi/\Phi_0 = 2eLd'B/\hbar$. Hence,

$$I_C = I_0\left|\frac{\sin(\chi/2)}{\chi/2}\right| \tag{11}$$

Following the above, the actual problem arising from Eq. (11) is how to solve the generalized model of the JJ, i.e., how to determine both the phase and the voltage with χ not being constant in time. Situations involving constant values of χ (therefore, constant values of I_c) are easy to be analyzed via specific software packages, such as JSPICE [58]. However, the problem regarding χ being a function of time cannot be analytically solved and a numerical solution for a non-integrable differential equation cannot be found out, too. Moreover, χ can exhibit any dependence on the variables of the system. To reach a solution, the user should manipulate the intrinsic FORTRAN code of JSPICE (similarly to other packages) and define new subroutines. This clearly represents an inconvenient. Even if possible, the optimization of the new subroutines is not evident at all. The same argument can be extended to the remaining parameters, C and R, in Eq. (7).

The NSM allows to compute the generalized RCSJ model with non-static parameters, no matter their dependence on time. Furthermore, the number of electric devices employed to solve the

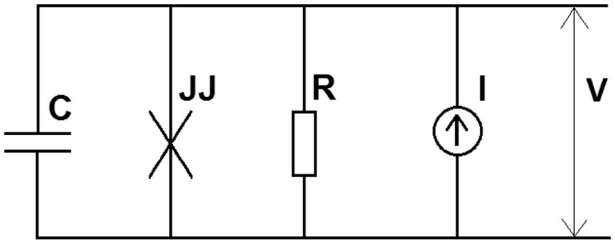

Fig. 1. Schematic diagram for the RCSJ.

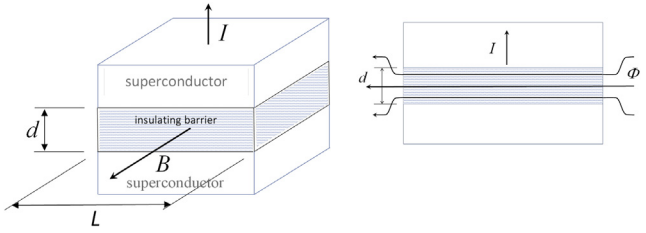

Fig. 2. Penetration of the magnetic field through the cross section in a JJ sample.

model remains the same: capacitors, resistors, and voltage-controlled current sources, as well. In this way, the novelty in this paper lies in the fact that the NSM can lead to solve the generalized RCSJ model following a similar approach as in the standard model, gaining advantage over other methods. The key here is to include in the main electrical network as many coupled auxiliary electrical circuits as new dependences.

According to Eq. (11), the generalized RCSJ model holds once Eq. (9) has been rewritten since R and C are assumed to be constants. To deal with, just replace I_0 by I_C. Also, an explicit expression containing the dependence of χ on time must be defined. For illustration purposes, next we provide an example regarding an alternate-like current dependence. In this case, the set of differential equations is as follows:

$$\begin{aligned} &A\sin(\omega\tau) = \tfrac{\mathrm{d}v}{\mathrm{d}\tau} + \gamma v + |\sin(\chi/2)/(\chi/2)|\sin\theta \quad (a)\\ &v = \tfrac{\mathrm{d}\theta}{\mathrm{d}\tau} \quad (b)\\ &\tfrac{\mathrm{d}\chi}{\mathrm{d}\tau} = 10\cos(\beta\tau) \quad (c) \end{aligned} \tag{12}$$

It is worth mentioning that Eq. (12) (c) has been chosen only from a mathematical viewpoint, though it has no applicative nature. Parameter β refers to an angular frequency, and pre-factor of 10 has been selected according to [55]. Interestingly, it holds that Eq. (12) (c) may exhibit a deep dependence on τ, so the problem does not increase in complexity from the NSM approach. In fact, this constitutes the main advantage of our procedure.

The network simulation method

The NSM establishes an equivalence between a mathematical model describing a physical transport process and electrical networks. Two main steps are required to properly apply that method: (i) to design a network associated to the system of differential equations describing the physical problem to be modeled, and (ii) to run the model in an appropriate circuit simulation code.

Regarding the first step, a general rule can be stated. Each differential equation in the mathematical model leads to an independent circuit, where each addend is considered as a current branch that is implemented in the network by an appropriate device. The branches are interconnected in such a way that the KCL is satisfied according to the sign of the addends in the equation. All the terms within a given equation are balanced as currents of different branches in a circuit node. For the whole problem, there will be as many circuits as equations, and for each equation, as many branches as addends. The NSM basically consists of finding the appropriate device for each addend in each differential equation and then properly connect them.

Only a few electrical devices are necessary to model the addends within the differential equations. They are of the following types:

(a) Capacitors: directly related to the first derivative addends, since the current i_C through a capacitor is defined as $i_c = C(\mathrm{d}V_c/dt)$. The voltage at its ends, V_C, is formally equal to the variable of the first derivative in the differential equation, known as the *node voltage*. The constant in front of the derivative is just the capacity C. Sometimes the differential equations are renormalized in such way that all the capacities are equal to one, as Eq. (13) establishes.

(b) Voltage-controlled current sources: related to addends, are functions of the node voltages. These devices are able to implement in the network any kind of linear or nonlinear addend given as a mathematical function of one or several dependent variables: the node voltages. To design such a device, it becomes necessary to implement the mathematical expression for each particular addend in the differential equation, and hence, to establish the direction of the current: if the sign of the addend is positive (resp. negative) the current will be outgoing (resp. incoming).

(c) Resistors: required by the computational code only to satisfy the continuity criteria, are usually chosen with very high values.

It is worth noting that only these three kinds of devices are employed to design the electrical networks. As a consequence, only a very few programming rules will be required to be implemented on a circuit software. To conclude the model, we have to design one electrical circuit per differential equation, and then they have to be connected to a common node. In most cases, that node is chosen as the ground. After this step, we only need to set the initial voltages of the capacitors.

For illustration purposes, let us apply the NSM to Eq. (12) (a), rewritten in terms of the KCL as follows:

$$\frac{\mathrm{d}v}{\mathrm{d}\tau} + \gamma v + \left|\frac{\sin(\chi/2)}{(\chi/2)}\right|\sin\theta - A\sin(\omega\tau) = 0 \tag{13}$$

The expression above has four addends, and hence, it has to be implemented by a circuit having four branches plus the resistor current branch, as shown in Fig. 3. This represents the generalized RCSJ model. The currents of these branches, $\mathrm{d}v/\mathrm{d}\tau$, $A\sin(\omega\tau)$,$|\sin(\chi/2)/(\chi/2)|\sin\theta$, and γv, are balanced at a common node (named v), according to their algebraic sign. Let us choose the positive addends as outgoing currents, flowing from the node to the ground. Observe that the first addend in Eq. (13) has been modeled by a 1F-capacitor. The voltage at the node (or equivalently, the voltage at the capacitor) is just the value of the unknown variable v.

The rest of the addends can be easily implemented via voltage-controlled current sources, which continuously read the values of the other nodes of the network, and operate adequately into the source to provide the required current output.

The addend $|\sin(\chi/2)/(\chi/2)|\sin\theta$ is implemented by the current source G_{v1}, whose output current, of value $|\sin(\chi/2)/(\chi/2)|\sin\theta$, can be read from the voltages θ and χ at the corresponding nodes in the network model. The same procedure can be applied to implement the addends γv (source G_{v2}) and $A\sin(\omega\tau)$ (source G_{v3}), whose outputs currents are obtained from the variable time τ, and the voltage node v, respectively.

Fig. 3 also illustrates the design regarding both Eqs. (12)(b) and (c). Thus, the whole model consists of three main circuits containing two nodes each: a common node (the circuit ground) and an

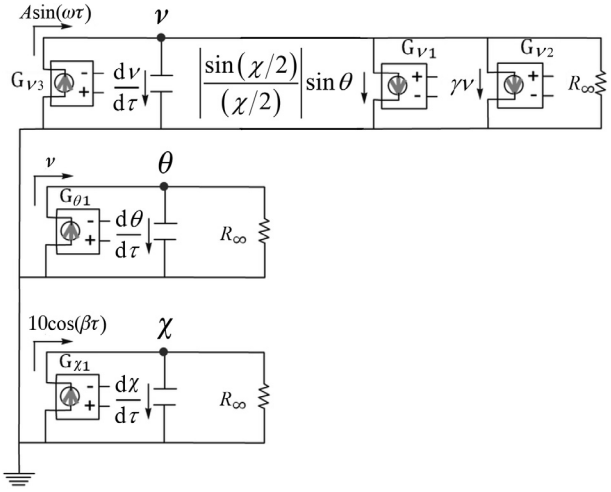

Fig. 3. Equivalent electrical circuit to Eq. (12) for the generalized RCSJ.

independent node, whose voltage is an unknown variable. The initial conditions are implemented by fixing the initial voltage of the capacitors.

In particular, for the standard JJ model, only two circuits have been used (see Eq. (9)).

Once the network model has been designed, the second step, namely, the circuit simulation, is carried out by a circuit code, such as PSpice [59], without any additional mathematical requirements. In our simulations we have employed OrCAD PSpice 9.2. An auxiliary C# program has been designed to import the tabulated data of PSpice code and also to represent them in MATLAB or Origin, for instance.

It is worth mentioning that no mathematical manipulations are further required since the simulation software carries out both the work related to the topological structure of the model (inherent in KCL) as well as the work related to the numerical solution, for which the algorithms implemented in the circuit simulation software are applied [60].

This constitutes one of the key advantages of the NSM. Further, the model becomes efficient, versatile, and computationally fast. Since one of the chaos indicators in dynamical systems, the Fast Fourier Transform [27] is easy to be handled in PSpice, we shall apply the NSM approach to test for chaos presence in both the standard and the generalized RSCJ, and also to carry out an analysis regarding the trajectories of the phase space. The obtained numerical results will be compared with those from 4th order Runge-Kutta (RK) algorithm.

The Fast Fourier Transform of the phase signal

In this subsection, we provide a brief sketch regarding the Fast Fourier Transform (FFT, hereafter) as well as other techniques usually applied in literature to deal with chaos detection.

A wide variety of analytic tools are available to test for chaotic behavior in dynamical systems. In this way, Lyapunov (characteristic) exponent, fractal dimension, and Fast Fourier Transform can be quoted, among others. In this paper, though, we shall focus on the FFT for numerical calculations.

FFT allows a non-periodic signal to be decomposed into harmonic (resp. sinusoidal) signals. Let us assume that a given periodic (resp. non-periodic) signal can be expressed in the following terms [61]:

$$F(t) = \int_{-\infty}^{+\infty} g(t)\exp(-i2\pi ft)\mathrm{d}t \tag{14}$$

where f denotes frequency, and $\exp(-i2\pi ft) = \cos(2\pi ft) - i\sin(2\pi ft)$, as usual. However, in empirical applications, we shall consider a discrete version of Eq. (14), namely,

$$F(v) = \frac{1}{n}\sum_{\tau=0}^{n-1} g(t)\exp(-i2\pi ft) \tag{15}$$

where v refers to frequency, and n is the number of samples. Recall that the Fourier amplitude can be calculated as the square root of the sum of the squares of both real and imaginary parts. Additionally, Fourier phase is the arc tangent of the ratio between the imaginary part and the real part.

On the other hand, if the motion becomes periodic (resp., quasi-periodic), then the shape of the Fourier amplitude presents a set of narrow spikes and hence, it provides some evidence that the signal can be expressed in terms of a discrete set of harmonic functions. Moreover, near the chaos onset, a continuous distribution of frequencies may appear, whereas in any neighborhood of chaotic motion, the continuous spectrum may dominate those discrete spikes [42].

In addition, since the FFT allows to determine the frequencies that set up the function signal, it can be used to reveal the periodic or chaotic behavior of the signal. The power spectrum of a periodic signal presents a sharp peak at the signal frequency ω and its harmonics, as well. On the other hand, a quasi-periodic signal will show several frequency peaks as well as their lineal combinations. However, a chaotic signal is characterized by a continuous power spectrum.

Results and discussion

The solutions of the RCSJ model described in Eq. (9) for different values of the parameters and initial conditions have been computed via the NSM approach. It is worth pointing out that the simulations have been carried out via OrCAD PSpice 9.2. It contains an implementation which combines the trapezoidal method and the Gear methods, both of them of 2nd order with variable time-stepping. A variety of parameters has been selected in order to get both chaotic and non-chaotic behaviors. It is worth noting that the discussion regarding the phase diagrams in each case throws valuable information to test for chaos. In addition, the FFT for each case will also be explored to complete our analysis.

First of all, we have compared the results obtained from the NSM and the fourth-order RK method with fixed time-stepping, respectively, for a prototypical case, by choosing the parameters $A = 1$, $\gamma = ½$, and $\omega = 2/3$ [62]. In this case, we have considered the initial conditions $\theta = 0$ and $\mathrm{d}\theta/\mathrm{d}\tau = 1$, as well. Fig. 4 (a) shows the trajectory of the phase difference θ vs. time τ for the solution obtained via the NSM (straight line), and the fourth-order Runge-Kutta (RK) algorithm [63] (empty dots), resp., with time ranging from $\tau = 0$ to $\tau = 60$. Moreover, the average difference (error) between both methods, computed in the range from 50 to 500, is equal to 0.15%.

Fig. 4 (b) shows the FFT transform of the solution. In this way, it is worth mentioning that PSpice can analyze multifrequency inputs and quickly obtain their FFT spectrum for upcoming analysis. Such a graphical representation shows a peak at $\omega = 0.106$ with an amplitude equal to 2.71 (dimensionless). That angular frequency corresponds to the frequency of the phase difference in the stationary state shown in Fig. 4 (a). The presence of a clear and sharp frequency peak constitutes a strong indicator of chaos absence.

Fig. 5 (a) shows phase θ vs. its derivative $\mathrm{d}\theta/\mathrm{d}\tau$, namely, its phase space under the same parameters as above. It is worth mentioning that phase space plots become quite useful to analyze complex oscillations, especially those that could behave chaotically. However, in non-chaotic contexts (like this one) the trajectory resembles an elliptical orbit repeating itself continuously, since it returns to the same point under the same conditions: in this case, with a 3π-period, the main frequency in the FFT plot.

On the other hand, Fig. 5 (b) contains the same information regarding the FFT as in Fig. 4 (in logarithmic scale). In addition to the main peak, that graphical representation shows two lesser peaks, at 0.318 and 0.53 (3 and 5 times the original, resp.) whose amplitudes are equal to 0.108 and 0.00866 (1/25 and 1/64 of the original, resp.). They are related to the thickness of the orbit, which does not strictly follow the same trajectory for each loop before returning to the starting point. The rest of the peaks appeared in that figure correspond to the initial transitory, disappearing once the first 2000 points have been removed. Again, the presence of sharp and clear frequency peaks throws information regarding chaos absence.

Fig. 6 (a) shows the results for the same parameter choice as in the previous simulation, but letting $A = 1.07$. The initial conditions have been chosen to be $\theta = 0$ and $\mathrm{d}\theta/\mathrm{d}\tau = 1$, resp. In this case, though, the phase space shows an orbit doubling. Thus, the elliptical orbit becomes periodic but repeats itself with a 6π-period,

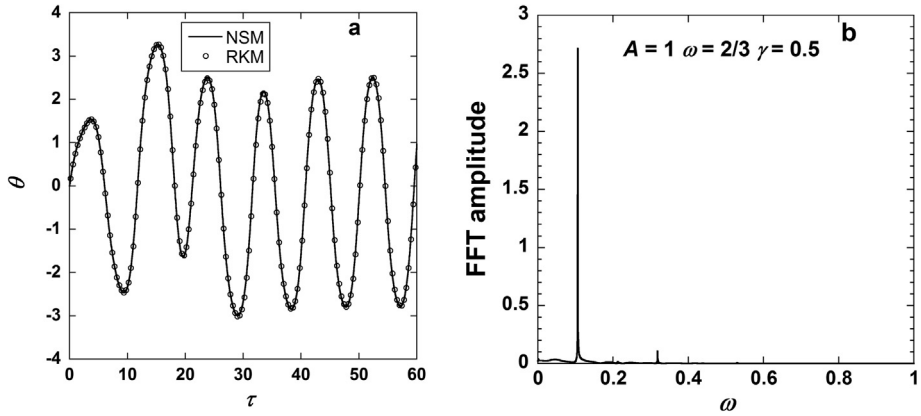

Fig. 4. (a) Phase vs. time by RCSJ model via the NSM (solid line), and by a fourth order Runge-Kutta algorithm (empty dots), as well. The parameter values are chosen to be $A = 1$, $\gamma = ½$, and $\omega = 2/3$. (b) FFT transform for θ vs. ω, only having a sharp peak at $\omega = 0.106$.

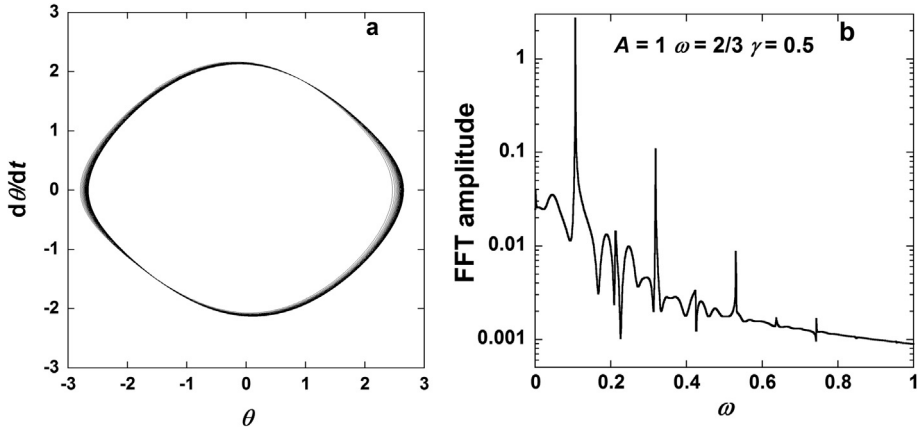

Fig. 5. (a) A periodic orbit under the same parameters as in Fig. 4. The first 2000 points have been removed from the plot since the trajectory is not periodic from the beginning. (b) The same FFT as in Fig. 3 (b), though a logarithmic rate has been considered in vertical axis, instead. Observe that several lesser peaks do appear.

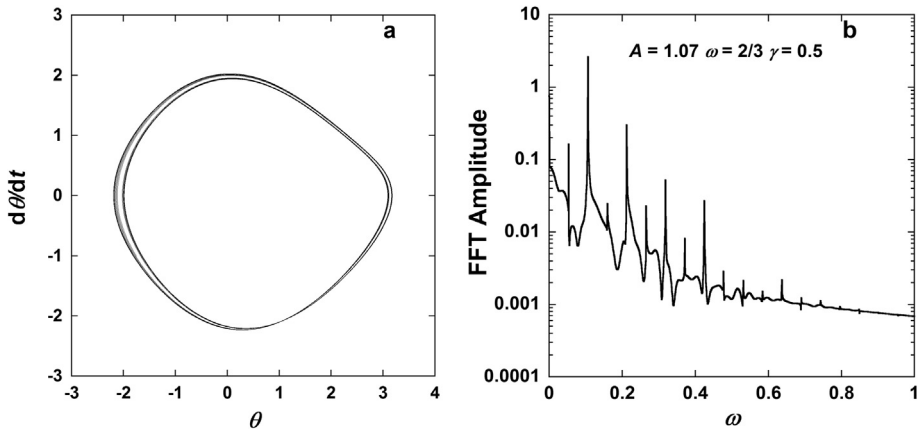

Fig. 6. (a) Similar representation to Fig. 5 for parameters values $A = 1.07$, $\gamma = ½$, and $\omega = 2/3$. The new trajectory shows a doubling orbit, since it does not return to the initial conditions until it completes two full orbits. In this case, the first 2300 points have been removed. (b) FFT of the trajectory.

having two close orbits instead of only one. Orbit doubling (also called as *period doubling*) is a phenomenon that occurs in nonlinear systems as amplitude A increases, and consists of a bifurcation (or branching) of the original loop as the number of iterations (or time) required to return to the original state doubles. There can be two, three or more bifurcations in an infinite sequence of orbit doubling as A increases. For higher values of A, the number of bifurcations grows after increasingly smaller increments (sixth decimal place variations). If the number of bifurcations is infinite, then the system behaves chaotically, namely, a region in which the phase trajectory has no apparent order and looks erratic [27]. It is worth mentioning that our method is precise enough to determine the range of A values for each zone and to discriminate their starting value up to 10 decimal digits, as well.

Fig. 6 (b) contains the FFT of this phase space. This presents a main peak at $\omega = 0.106$ with an amplitude equal to 2.62. Observe that this is the same angular frequency as in Fig. 5, though in this case, the second and third peaks appear at $\omega = 0.212$ and $\omega = 0.318$, resp., namely, twice and thrice the main frequency, resp. Further, the amplitudes of these peaks are 0.299 (1/9 of the first one), and 0.052 (1/50 of the original), respectively. These peaks are only related to the thickness of the orbits. The remaining peaks correspond to the initial transitory state and disappear once the first 2300 points have been removed.

On the other hand, if the amplitude is further increased to $A = 1.5$, letting $\gamma = 1/2$ and $\omega = 2/3$, then the chaotic zone is reached, leading to the trajectory provided in Fig. 7 (a), where the initial conditions are $\theta = 0$ and $d\theta/d\tau = 1$, and the phase diagram has been displayed along the interval $(-\pi, \pi)$. No periodic orbit is ever repeated, which is a strongly indicative that the system behaves chaotically.

Fig. 7 (b) presents its corresponding FFT, where the intrinsic chaotic nature is also revealed due to a continuous noise spectrum, despite it shows again two main peaks at $\omega = 0.106$ and $\omega = 0.318$, resp., the same frequencies as in original non-chaotic Fig. 4, since this frequency depends on the forced frequency parameter ω.

Fig. 5 (a) shows the phase space trajectory by parameters $A = 0.9045$, $\gamma = ½$, and $\omega = 0.47$ [60], and initial conditions $\theta = 0$ and $d\theta/d\tau = 0$. It depicts an interesting phenomenon regarding the chaotic behavior of the JJ. The plot presents regular oscillations with no orbit doubling, connected with chaotic and repetitive 2π or 4π phase jumps. They are related to turbulent bursts in the voltage along the junction, giving rise to the so-called *intermittency chaos*. Intermittency is a complex steady-state considered as a route to chaos different from orbit doubling and, in most cases, is the only empirically observable chaos in JJ [64].

The FFT characteristic of this phenomenon is shown in Fig. 8b, where its chaotic nature is revealed again via an almost continuous spectrum of noise frequencies up to 0.6, approximately. At any rate, it presents two peaks, located at $\omega = 0.075$ and $\omega = 0.224$, respectively. These peaks are quite different from those in the previous figures though the connection with the new frequency ω still remains.

The generalized RCSJ model also presents some interest from an experimental viewpoint [53–57], and constitutes a more complex situation where numerical simulations are still scarce. Next we show the results thrown by the NSM applied to Eqs. (12). To study the influence of the parameter β, we have chosen$A = 0.2$, $\gamma = 0.5$ and $\omega = 2/3$. Hence, in absence of an external magnetic field, a periodic orbit can be found in the standard RCSJ model (similarly to both Figs. 4 and 5). The dynamics in Eqs. (12) become richer and more complex as a consequence of varying β. More especifically, for smaller values of β (< 0.05), several chaotic trajectories appear, whereas for $\beta > 5$, the system recovers the standard model behavior.

In Fig. 9 they have been shown the phase diagrams for different values of β in the generalized RCSJ model. From the analysis of the FFT, we have determined that the graphical representations from

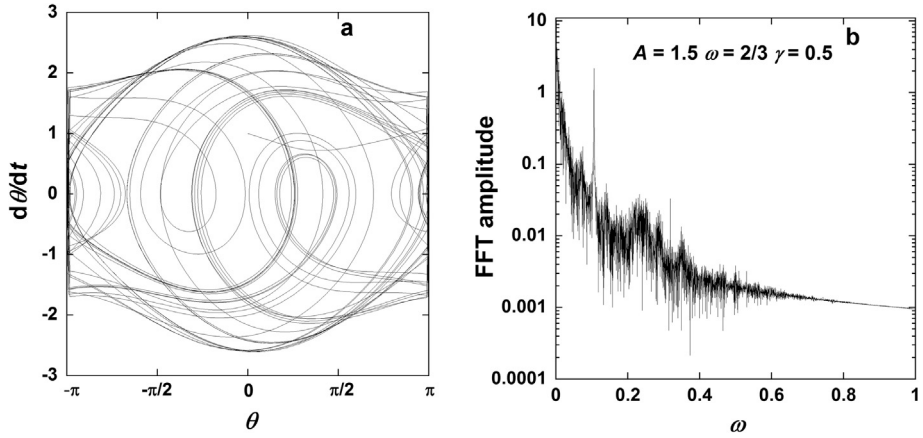

Fig. 7. (a) Chaotic trajectory in a graphical representation for $d\theta/d\tau$ vs. θ In this case, the parameters have been chosen to be $A = 1.5$, $\gamma = ½$, and $\omega = 2/3$. (b) FFT of the trajectory.

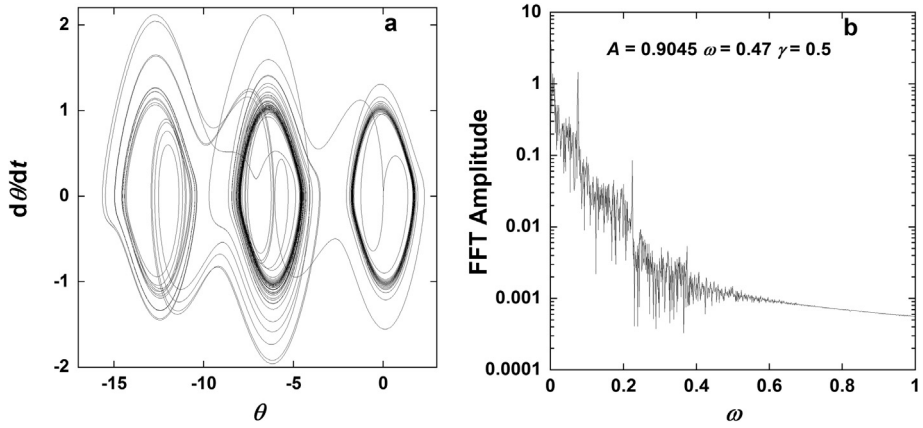

Fig. 8. (a) The *intermittency* phenomenon. The plot shows $d\theta/d\tau$ vs. θ for parameter choice $A = 0.9045$, $\gamma = 0.5$, and $\omega = 0.47$. (b) FFT of the trajectory.

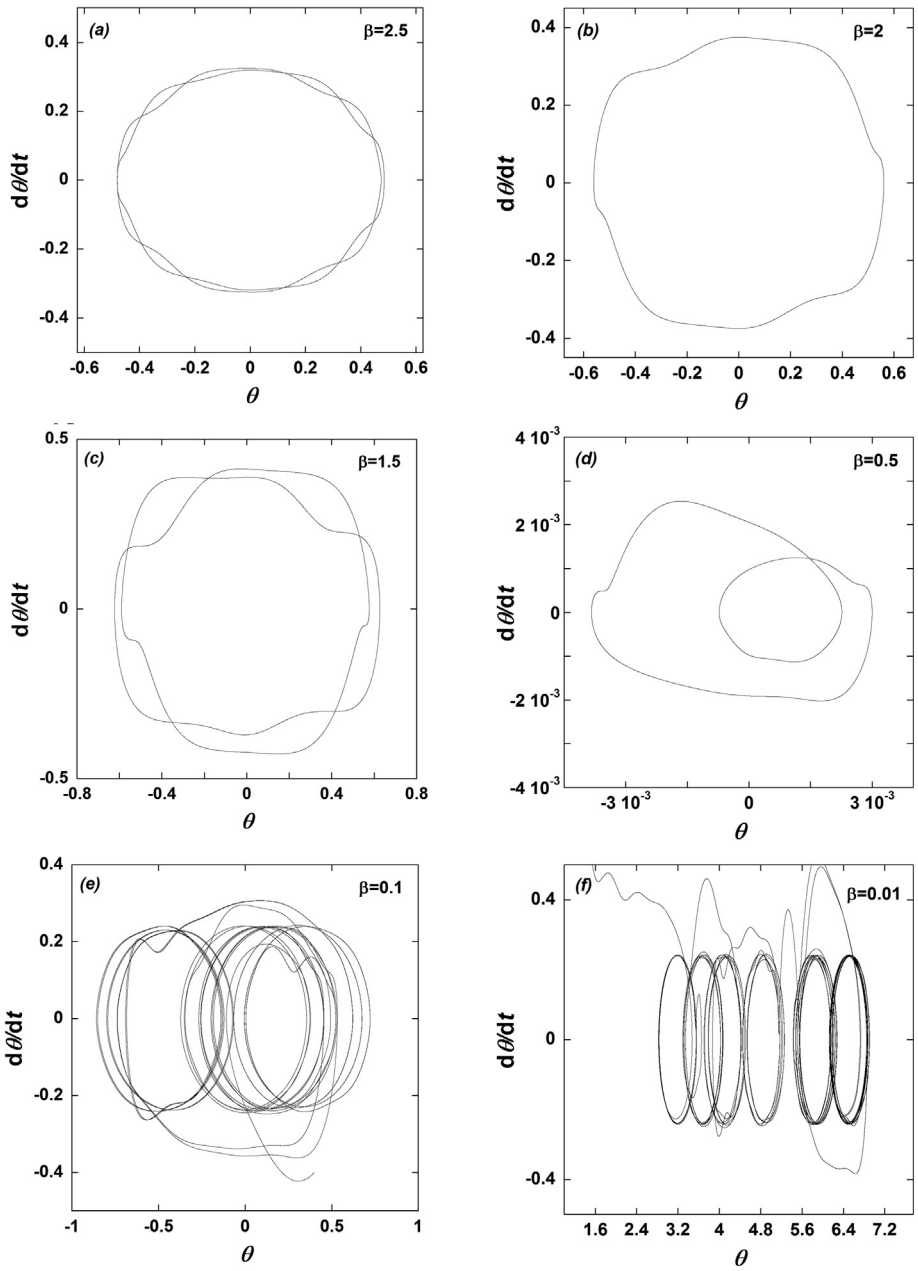

Fig. 9. Phase diagrams for the generalized RCSJ model. The parameters are $A = 0.2$, $\gamma = 0.5$, and $\omega = 2/3$, and the initial conditions and β values have been chosen as follows: (a) $\theta = -0.39$, $d\theta/d\tau = 0.19$, $\beta = 2.5$; (b) $\theta = -0.541$, $d\theta/d\tau = 0.133$, $\beta = 2$; (c) $\theta = -0.621$, $d\theta/d\tau = -0.048$, $\beta = 1.5$; (d) $\theta = -0.00025$, $d\theta/d\tau = -0.0018$, $\beta = 0.5$; (e) $\theta = 0.0013$, $d\theta/d\tau = -0.0018$, $\beta = 0.1$; (f) $\theta = 1.2$, $d\theta/d\tau = 0.4$, $\beta = 0.01$.

(a) to (d) do present periodic behavior, while (e) and (f) display chaotic dynamics. Additionally, plot (f) shows again intermittency.

As Fig. 5-Fig. 9 point out, the NSM allows to compute the phase diagram and the FFT of different chaotic and non-chaotic behavior mechanisms, having an excellent accuracy and being fast enough compared to other classical numerical methods. Its simplicity and calculation power makes it a pretty good alternative to deal with the chaotic behavior in dynamical systems.

Conclusions

In this work, resistively and capacitively shunted Josephson junctions (RCSJ) have been numerically explored via a network model whose design is based on the so-called Network Simulation Method (NSM). This approach takes advantage from the powerful algorithms implemented in a circuit simulation software. Since the NSM is based on the formal equivalence between physical systems and electrical networks, it has been applied in problems of great mathematical complexity in science and engineering.

The approach presented along this paper becomes efficient, versatile and computationally fast. It does not need the mathematical manipulations inherent to other numerical methods, since this work is carried out entirely by the circuit code. Moreover, it is also worth mentioning that the implemented circuit only contains a few electrical devices. Thus, only a very few programming rules depend on the user handling.

The Resistively and Capacitively Shunted Josephson Junction (RCSJ) device provides a valuable test to explore chaos in dynamical systems. In this way, we show that the NSM becomes a simple

and useful tool to address that problem. Moreover, as a novel application, we deal with the generalized RCSJ model, under the assumption that the critical current depends on an external magnetic field. Interestingly, the solution we contribute presents even more complex nonlinear dynamics.

Additionally, a wide range of parameters has been selected to obtain different and characteristic both chaotic and non-chaotic behaviors. In this way, the numerical results obtained via the NSM have been compared with those from other standard numerical approaches in order to check out the reliability of such an electrical procedure. We would like also to highlight the easiness when obtaining both phase diagrams and FFT plots, which throw some useful information regarding the presence of chaos.

Overall, due to its generality and flexibility, we can conclude that the application of the NSM electrical equivalence presents an actual usefulness from the point of view of the circuit theory and its subsequent applications, as well.

Acknowledgments

The last three authors would like to thank Research Projects MTM2014-51891-P from Spanish Ministry of Economy and Competitiveness and 19219/PI/14 from Fundación Séneca de la Región de Murcia for their partially support. The authors would like to express their gratitude to anonymous reviewer whose insightful comments and suggestions have allowed us to enhance the quality of this paper.

References

[1] Marion JB. Classical dynamics of particles and systems. Academic Press; 2013.
[2] Goldstein H. Classical mechanics. Pearson Education India; 1965.
[3] Horno Montijano J. Network simulation method. Research Signpost; 2002.
[4] Anderson PW, Chapter I. The josephson effect and quantum coherence measurements in superconductors and superfluids. In: Gorter CJ, editor. Progress in low temperature physics. Elsevier; 1967. p. 1–43.
[5] Vavalis M, Mu M, Sarailidis G. Finite element simulations of window Josephson junctions. J Comput Appl Math 2012;236:3186–97.
[6] Clarke J. A superconducting galvanometer employing Josephson tunnelling. Phil Mag 1966;13:115–27.
[7] Yang X-S, Li Q. A computer-assisted proof of chaos in Josephson junctions. Chaos, Solitons Fractals 2006;27:25–30.
[8] Song I, Kang K-Y, Park G. Frequency-locked submillimeter wave generation from Josephson junction arrays. Jpn J Appl Phys 1999;38:44–7.
[9] Zhang LS, Cai L, Feng CW. Quantitative calculation and bifurcation analysis of periodic solutions in a driven Josephson junction including interference current. Phys C 2011;471:150–5.
[10] Uçar A, Lonngren KE, Bai E-W. Chaos synchronization in RCL-shunted Josephson junction via active control. Chaos, Solitons Fractals 2007;31:105–11.
[11] Pedersen NF. Non-linear properties of Josephson junctions. Phys D 1993;68:27–34.
[12] Wang C, Chu R, Ma J. Controlling a chaotic resonator by means of dynamic track control. Complexity 2014;21(1):370–8.
[13] He D-R, Yeh WJ, Kao YH. Studies of return maps, chaos, and phase-locked states in a current-driven Josephson-junction simulator. Phys Rev B 1985;31:1359–73.
[14] Ma J, Wu X, Chu R, Zhang L. Selection of multi-scroll attractors in Jerk circuits and their verification using Pspice. Nonlinear Dyn 2014;76:1951–62.
[15] Kautz RL, Monaco R. Survey of chaos in the rf-biased Josephson junction. J Appl Phys 1985;57:875–89.
[16] D'Humieres D, Beasley MR, Huberman BA, Libchaber A. Chaotic states and routes to chaos in the forced pendulum. Phys Rev A 1982;26:3483–96.
[17] Lorenz EN. Deterministic nonperiodic flow. J Atmos Sci 1963;20:130–41.
[18] Shahverdiev EM, Hashimova LH, Bayramov PA, Nuriev RA. Chaos synchronization between josephson junctions coupled with time delays. J Supercond Novel Magn 2014:1–5.
[19] Perc M. Visualizing the attraction of strange attractors. Eur J Phys 2005;26:579.
[20] Mariño IP, López L, Sanjuán MAF. Channel coding in communications using chaos. Phys Lett A 2002;295:185–91.
[21] Pecora LM, Carroll TL. Synchronization in chaotic systems. Phys Rev Lett 1990;64:821–4.
[22] Hasler M. Synchronization of chaotic systems and transmission of information. Int J Bifurcation Chaos 1998;08:647–59.
[23] Short KM. Signal extraction from chaotic communications. Int J Bifurcation Chaos 1997;07:1579–97.
[24] Epaminondas Rosa J, Hayes S, Grebogi C. Noise filtering in communication with chaos. Phys Rev Lett 1997;78:1247–50.
[25] Mariño IP, Rosa E, Grebogi C. Exploiting the natural redundancy of chaotic signals in communication systems. Phys Rev Lett 2000;85:2629–32.
[26] Sugiura T, Yamanashi Y, Yoshikawa N. Demonstration of 30 Gbit/s generation of superconductive true random number generator. IEEE Trans Appl Supercond 2011;21:843–6.
[27] Bergé P, Pomeau Y, Vidal C. Order within chaos. Wiley and Sons; 1984.
[28] Kurt E, Canturk M. Chaotic dynamics of resistively coupled DC-driven distinct Josephson junctions and the effects of circuit parameters. Phys D 2009;238:2229–37.
[29] Duzer TV, Turner CW. Principles of superconductive devices and circuits. Prentice Hall; 1999.
[30] Borcherds PH. A computational study of some Josephson junction circuits. Comput Phys Commun 2002;147:87–90.
[31] Blackburn JA, Smith H, Gro N, et al. Resonant steps in the characteristics of a Josephson junction coupled to a transmission line. J Appl Phys 1991;70:2395–401.
[32] Vincent U, Ucar A, Laoye J, Kareem S. Control and synchronization of chaos in RCL-shunted Josephson junction using backstepping design. Phys C 2008;468:374–82.
[33] Peusner L. The principles of network thermodynamics: theory and biophysical applications. Entropy 1987.
[34] Zueco J, Campo A. Network model for the numerical simulation of transient radiative transfer process between the thick walls of enclosures. Appl Therm Eng 2006;26:673–9.
[35] González-Fernández CF, García-Hernández MT, Horno J. Computer simulation of a square scheme with reversible and irreversible charge transfer by the network method. J Electroanal Chem 1995;395:39–44.
[36] Zueco J, Alhama F, González Fernández CF. Inverse problem of estimating time-dependent heat transfer coefficient with the network simulation method. Commun Numer Methods Eng 2005;21:39–48.
[37] Castro E, García-Hernández MT, Gallego A. Transversal waves in beams via the network simulation method. J Sound Vib 2005;283:997–1013.
[38] Caravaca M, Sanchez-Andrada P, Soto A, Alajarin M. The network simulation method: a useful tool for locating the kinetic–thermodynamic switching point in complex kinetic schemes. Phys Chem Chem Phys 2014;16:25409–20.
[39] Soto Meca A, Alhama López F, González Fernández C. Density-driven flow and solute transport problems. A 2-D numerical model based on the network simulation method. Comput Phys Commun 2007;177:720–8.
[40] Alhama I, Alhama F, Soto Meca A. The network method for a fast and reliable solution of ordinary differential equations: Applications to non-linear oscillators. Comput Electr Eng 2012;38:1524–33.
[41] Soto Meca A, Alhama F, González Fernández CF. An efficient model for solving density driven groundwater flow problems based on the network simulation method. J Hydrol 2007;339:39–53.
[42] Moon FC. Chaotic and fractal dynamics: introduction for applied scientists and engineers. John Wiley & Sons; 2008.
[43] Finger L. The Josephson junction circuit family: network theory. Int J Circuit Theory Appl 2000;28:371–420.
[44] McCumber D. Effect of ac impedance on DC voltage-current characteristics of superconductor weak-link junctions. J Appl Phys 1968;39:3113–8.
[45] Stewart W. Current-voltage characteristics of Josephson junctions. Appl Phys Lett 1968;12:277–80.
[46] Whan CB, Lobb CJ. Complex dynamical behavior in RCL-shunted Josephson tunnel junctions. Phys Rev E 1996;53:405–13.
[47] Dana SK, Sengupta DC, Edoh KD. Chaotic dynamics in Josephson junction. IEEE Trans Circuits Syst I 2001;48:990–6.
[48] Makhlin Y, Schön G, Shnirman A. Quantum-state engineering with Josephson-junction devices. Rev Mod Phys 2001;73:357–400.
[49] Gallop JC. SQUIDs, the Josephson effects and superconducting electronics. CRC Press; 1991.
[50] Abellán FJ, Ibáñez JA, Valerdi RP, García JA. The Stefan-Boltzmann constant obtained from the I-V curve of a bulb. Eur J Phys 2013;34:1221.
[51] Jensen KF, Hirai T, Wahl G, Pauleau Y. Chemistry for electronic materials. Elsevier; 1993.
[52] Kurzweil P, Frenzel B, Hildebrand A. Voltage-dependent capacitance, aging effects, and failure indicators of double-layer capacitors during lifetime testing. ChemElectroChem 2015;2:160–70.
[53] Fiske M. Temperature and magnetic field dependences of the josephson tunneling current. Rev Mod Phys 1964;36:221–2.
[54] Altshuler E, Garcıa R. Josephson junctions in a magnetic field: Insights from coupled pendula. Am J Phys 2003;71:405–8.
[55] Wollman D, Van Harlingen D, Giapintzakis J, Ginsberg D. Evidence for d x 2−y 2 Pairing from the Magnetic Field Modulation of Y Ba 2 Cu 3 O 7-Pb Josephson Junctions. Phys Rev Lett 1995;74:797.
[56] Rowell JM. Magnetic Field Dependence of the Josephson Tunnel Current. Phys Rev Lett 1963;11:200–2.
[57] Watanabe N, Nakayama A, Abe S, Aizawa K. Magnetic field dependence of Josephson current by applying the external magnetic field perpendicular to the Josephson junction. J Appl Phys 2005;97. 10B116–10B116.
[58] Jewett R. Josephson junctions in SPICE 2G5. Berkeley, CA, 94720: Electronics Research Lab internal memoranda, Department of Electrical Engineering and Computer Sciences, University of California; 1982.
[59] Blume W. PSpice circuit Simulator. MicroSim; 1984.

[60] Korsch HJ, Jodl H-J, Hartmann T. Chaos: a program collection for the PC. Springer Science & Business Media; 2007.
[61] Bracewell RN. The fourier transform. Sci Am 1989;260:86–95.
[62] Timilsina R. Chaotic dynamics of a driven pendulum. University of Southern Mississippi.
[63] Press WH. Numerical recipes 3rd edition: the art of scientific computing. Cambridge University Press; 2007.
[64] Gwinn E, Westervelt R. Intermittent Chaos and Low-Frequency Noise in the Driven Damped Pendulum. Phys Rev Lett 1985;54:1613–6.